THE ROLE OF PHYLLOSILICATE PARTIAL MELTING IN SEGREGATING W AND Sn DEPOSITS IN W-Sn METALLOGENIC PROVINCES

Panlao Zhao[1,2,3], Xu Chu[3], Anthony E. Williams-Jones[4], Jingwen Mao[1], Shunda Yuan[1*]

1. China University of Geosciences, Beijing 100083, China

2.MLR Key Laboratory of Metallogeny and Mineral Assessment, Institute of Mineral Resources, Chinese Academy of Geological Sciences, Beijing 100037, China

3. Department of Earth Sciences, University of Toronto, 22 Ursula Franklin Street, Toronto, Ontario M5S 3B1, Canada

4. Department of Earth and Planetary Sciences, McGill University, 3450 University Street, Montreal H3A 0E8, Canada

ABSTRACT

Most W and Sn deposits are associated with highly-evolved granites derived from the anatexis of metasedimentary rocks. They are commonly separated in both space and time and in the rare cases where the W and Sn mineralization is part of a single deposit, the two metals are temporally separate. The factors controlling this behavior, however, are not well understood. A compilation of whole-rock geochemical data for W- and Sn-related granites in major W-Sn metallogenic belts presented in this study shows that the Sn-related granites are generally the products of higher temperature partial-melting (~800 ^{o}C) than the W-related granites (~750 ^{o}C). Thermodynamic modeling of partial melting and metal partitioning shows that W is incorporated into the magma formed during low-temperature muscovite-dehydration melting, whereas most of the Sn is released into the magma at a higher temperature during biotite-dehydration melting; the Sn of the magma may be increased significantly if melt is extracted prior to biotite melting. At the same degree of partial melting, the concentrations of the two metals in the partial melt are controlled

Zhao, P., Chu, X., Williams-Jones, A. E., Mao, J., and Yuan, S., 2022,
The role of phyllosilicate partial melting in segregating tungsten and tin deposits in W-Sn metallogenic provinces:
Geology, v. 50, p. 121-125.

by their concentration in the protolith. Thus, the nature of the protolith, the melting temperature and the subsequent evolution of the magma all influence the metallogenic potential of a magma and, in combination, helped control the spatial and temporal segregation of W and Sn deposits in all major W-Sn metallogenic belts.

INTRODUCTION

The bulk of the World's W and Sn resources are hosted by magmatic-hydrothermal ore deposits associated with granitic intrusions of S-type affinity (Lehmann, 1990; Brown and Pitfield, 2014). Owing to their highly incompatible behavior, W and Sn are enriched in the continental crust and in highly evolved granitic magmas derived from the partial melting of metapelitic rocks (Ishihara, 1977; Romer and Kroner, 2016; Gardiner et al., 2017). These magmas are widely considered to be the sources of the mineralizing fluids that lead to W and Sn deposits (Audétat, 2019). Despite the similar geochemical behavior of W and Sn during fractional crystallization, a spatial or temporal coexistence of deposits containing the two metals is rare (Fig. 1). Among major deposits, only 3 of 77 W- or Sn-bearing skarn deposits in China (Chang et al., 2019) and 6 of 69 in the Bolivian Sn belt contain significant concentrations of both W and Sn (Clark et al., 1990; Mlynarczyk and Williams-Jones, 2005; Arce-Burgoa and Goldfarb, 2009). Previous studies have generally attributed the decoupling of W and Sn mineralization to the compositions of the granites, the degree of fractionation and the redox state (Blevin and Chappell, 1992, 1995; Lehmann, 2020). Most W and Sn deposits, however, are associated with highly evolved, reduced or ilmenite-series granites (Ishihara, 1977; Lehmann, 1990; Lecumberri-Sanchez et al., 2017; Yuan et al., 2019) and the reasons for their separation is still not well- understood.

Although partial melting and fractional crystallization have similar effects on the formation of W-Sn deposits (Simons et al., 2017; Yuan et al., 2019), most previous studies have emphasized the latter to explain the segregation of W and Sn mineralization in W-Sn metallogeny (Lehmann, 1990, 2020; Blevin and Chappell, 1992, 1995). Recently, Yuan et al. (2019) concluded that the spatial separation of W and Sn mineralization in the Nanling W-Sn metallogenic belt, South China might be related to differences in the melting temperature of the related granites i.e., that W-related granites were the products of low melting temperature <750 °C, whereas the Sn-related granites crystallised from magmas produced at T >800 °C. A similar conclusion was reached by Simons et al. (2017) from a study of the deposits associated with the Cornubian Batholith in SW England. However, although there is circumstantial evidence to support this hypothesis, acceptance of the notion of melting-induced W-Sn fractionation will require quantitative evaluation.

In this study, we use a quantitative partial melting model in concert with a compilation of published whole-rock geochemical data for W- and Sn-related granites in the major W and Sn metallogenic belts of the World to discuss how partial melting contributes to the enrichment of W and Sn in S-type granitic magmas (Fig. 1). The results show that the enrichment of W and Sn in the protolith and the dehydration partial melting of muscovite and biotite exert an important influence on subsequent W and Sn mineralization.

MAGMA TEMPERATURE AND THE DECOUPLING OF W AND Sn MINERALIZATION

The geochemical data for granites compiled here show clear genetic relationships between the granites and W or Sn deposits. Granites related to Cu-W and Mo-W deposits, which are usually oxidized (Mao et al., 2019), are not included in the compilation. The fractional crystallization indices, including bulk rock TiO_2, Nb/Ta, Zr/Hf, and Rb/Sr ratios, show that both W- and Sn-related granites are highly evolved (Fig. 2A and S1, Lehmann, 1990; Ballouard et al., 2016). The increase of the concentrations of both W and Sn with the degree of fractional crystallization (Fig. S3) is consistent with the coexistence of the W/Sn deposits and late-phase intrusions in large composite plutons (Lehmann, 1990). These mineralizing intrusions are classified as ilmenite series (reduced) granites and have overlapping Fe_2O_3/FeO ranges that indicate similar, low oxygen fugacity (Fig. 2A; Ishihara et al., 2000). Their Fe_2O_3/FeO ratios are largely independent of the fractionation indices (Fig. S4), suggesting reduced conditions inherited from the source regions (carbonaceous metasedimentary protolith; Burnham and Ohmoto, 1980; Lehmann, 1990). Therefore, magma evolution and redox state are insufficient to explain the separation of W and Sn mineralization in metallogenic belts.

As the initial temperatures of the magmas crystallizing W- and Sn-related granites are known to differ significantly (Yuan et al., 2019;), we used zircon-saturation thermometry (T_{Zr}; Watson and Harrison, 1983) to estimate the temperatures for the magmas related to the W- and Sn-granites considered in our compilation. However, because fractional crystallization is accompanied by cooling of the magma (Fig. S1), we used the highest temperature for a given granite to represent the initial temperature of the corresponding magma on the grounds that this would be the temperature for which the degree of fractional crystallization was lowest. The global compilation of T_{Zr} from the least evolved sample of each granite suite shows that Sn-related granites have systematically higher melting temperatures (~800 °C) than W-related granites (~750 °C; Fig. 2B). Furthermore, because inherited zircon cores are rare in Sn-related granites but common in W-related granites (Yuan et al., 2019; References in Table S1), the difference in the initial magma temperatures for W- and Sn-related granites might be even greater than estimated (Miller et al., 2003).

SEPARATION OF W AND SN DURING PARTIAL MELTING

In order to gain insight into how melting of a sedimentary protolith might affect the W and Sn contents of a granitic magma, we evaluated the partitioning of these elements between minerals and partial melt using a batch melting model. Using the mineral-melt partition coefficients for W and Sn (Table S2), we determined the concentrations of W and Sn in the melt from the W and Sn concentrations of the source rock, and the relative proportions of minerals and melt.

The mineral-melt partition coefficients of W and Sn are mainly from Simons et al. (2017) and this study (Table S2), and show that whereas W prefers muscovite strongly over the melt, the reverse is true for biotite, i.e., W prefers the melt more strongly than it does biotite. In contrast, Sn prefers both minerals over the melt, although the muscovite-melt partition coefficient for Sn is somewhat higher than the biotite-melt partition coefficient. The error introduced to the results of the modeling by errors in the partition coefficients is negligible (Fig. 3 and Supplementary Material 1).

The initial W and Sn concentrations are from unaltered Shuangqiaoshan Group metasedimentary rocks (C_W = 11.8 ppm, C_{Sn} = 21.4 ppm; Liu et al., 1982), which are considered to be the protolith of the W- and Sn-related granites in the South China W-Sn province (Su and Jiang, 2017). This choice of initial concentrations is consistent with the observation that W and Sn are enriched in the source metapelitic rocks in W-Sn metallogenic belts (Romer and Kroner, 2016). Similar fractionation trends of W and Sn were obtained using the W and Sn concentrations of bulk continental crust (1.0 ppm W, 1.7 ppm Sn; Rudnick and Gao, 2014).

The relative proportions of mineral and melt were obtained by modeling phase equilibria for average pelite (White et al., 2007) using THERMOCALC, along P-T paths from 650 to 1000 ^{o}C at pressures of 0.5, 0.7, and 0.9 GPa. The equilibrium phase assemblages along these P-T paths are shown in Figure 3 and Figure S2. Tungsten and Sn partition passively among the phases, and their concentrations do not affect the stabilities of the minerals.

Details of the methods employed in the modeling of batch melting are provided in Supplementary Material 1. The 0.5 GPa model is used as a representative to discuss the results of this modeling (Fig. 3, S2 and Table S3). The dehydration of muscovite within the supersolidus assemblage transfers water to the melt, generating a pulse of partial melting that is followed by a second pulse resulting from the melting of biotite at higher temperature (White et al., 2001). The enrichment of W and Sn in the melt correlates with a decrease in the fractions of W and Sn in muscovite and biotite, respectively (Fig. 3A2). The proportion of melt reached ~10 wt% after exhaustion of the muscovite at 680 °C, and the concentration of W reached a maximum of 49 ppm (Fig. 3A3). This represents a four-fold enrichment of W relative to its concentration in the protolith, and the release to the melt of approximately 41 wt% of the W in the protolith (Fig. 3A2). The W concentration in the melt then decreased (Fig. 3A3) in response to dilution by the next batch of melt, which is depleted in W. The decomposition of muscovite contributed minor Sn to the melt with only ~11 wt% of the protolith Sn being released. After the exhaustion of muscovite, the concentration of Sn in the melt increased and reached a maximum of 39 ppm at 854 °C. This maximum occurred after 51% partial melting when biotite was exhausted in the restite and 93 wt% of the bulk Sn had been released to the melt. If the melt had been removed from the source region shortly after the exhaustion of muscovite, subsequent biotite-dominated melting of the restite would have yielded a higher concentration of Sn (57 ppm; Fig 3B3). Thus, the main control on the concentration of W and Sn in a S-type granitic magma is the degree of partial melting, which depends largely on the temperature and much less on the pressure.

CONCENTRATION OF W AND SN DURING COMBINED PARTIAL MELTING AND FRACTIONAL CRYSTALLIZATION

Fractional crystallization amplifies the difference between W and Sn concentrations in magmas. These concentrations are important for the W-Sn mineralization potential, because elevated W and Sn concentrations in the exsolved magmatic-hydrothermal fluids are indicators of the type and extent of mineralization (Audétat, 2019). Here, we use a Rayleigh fractionation model to simulate the evolution of W and Sn concentrations during fractional crystallization (Fig. 4; methods described in Supplementary Material 1). The influence of restite is not considered as restite minerals are rare in W-Sn-related granites (Supplementary Material 1). We then compare the W and Sn concentrations to those of melt inclusions from W-Sn related granites (Audétat et al., 2000; Zajacz et al., 2008; Borisova et al., 2012; Fig. 4) to estimate the mineralizing potential of the magma.

Zhao, P., Chu, X., Williams-Jones, A. E., Mao, J., and Yuan, S., 2022,
The role of phyllosilicate partial melting in segregating tungsten and tin deposits in W-Sn metallogenic provinces:
Geology, v. 50, p. 121-125.

If the melt is generated by muscovite decomposition, C_W^{melt} reaches the W content in melt inclusions from W-Sn-related granites prior to extreme crystallization (10 wt% melt remaining, Ballouard et al., 2016; Fig. 4A). Nonetheless, fractional crystallization of this magma fails to concentrate C_{Sn}^{melt} sufficiently (Fig. 4A,). In contrast, if the melt is generated by biotite breakdown at high temperature (Fig. 4B), especially if there was prior extraction of melt after muscovite melting (Fig. 4C), the C_{Sn}^{melt} reaches the Sn content of melt inclusions from W-Sn-related granites. This, however, is not the case for C_W^{melt}. Therefore, the evolution of granitic magmas produced at low-temperature by muscovite-dehydration melting of a W-Sn-rich protolith is predicted to lead to granites generating W mineralization, and magmas produced at a higher temperature by biotite-dehydration melting are predicted to produce granites generating Sn mineralization. Magmas produced at intermediate temperature (e.g. ~790 ^oC), may be enriched in both W and Sn and might be responsible for the formation of deposits containing significant concentrations of both W and Sn. In the extreme, i.e., > 90 wt% of fractional crystallization, the low-temperature magma could potentially form W-dominated W-Sn deposits, and the high-temperature magma Sn-dominated Sn-W deposits.

In addition, we note that an enriched sedimentary protolith is also a prerequisite for the generation of W- and/or Sn- fertile melt. Otherwise, with an average continental crust protolith composition (1.0 ppm W and 1.7 ppm Sn; Rudnick and Gao, 2014), the residual melt would contain insufficient W and Sn after even 99% crystallization (Fig. 4).

IMPLICATIONS FOR MINERALIZATION ASSOCIATED WITH EXTREMELY FRACTIONED GRANITES

The model developed here shows that the temperature and degree of partial melting of an appropriate protolith determines whether the resulting granites will be fertile sources for economic W-Sn mineralization, something that has been largely overlooked in previous studies of W-Sn ore genesis (Romer and Kroner, 2016; Wolf et al., 2018). It is also possible that analogous temperaturesensitive incongruent partial melting might play an important role in the formation of deposits of other metals, e.g. Ta-, Li-, and Be-deposits, which like those of W and Sn, are genetically related to highly evolved S-type granites (Romer and Kroner, 2016). Indeed, it is noteworthy that among the protolith minerals that might act as potential sources for these metals, the mineral-melt partition coefficients of Ta and Li are highest for biotite and that of Be is highest for muscovite and cordierite (Simons, et al., 2017; Table S2). Thus, the behaviour of these metals during partial melting is a topic that merits further investigation and could provide new insights into the genesis of other types of metallic mineral deposits associated with reduced S-type granites.

ACKNOWLEDGEMENTS

This research was supported financially by the National Natural Science Foundation of China (41822304, 41672095). We thank editor, Gerald Dickens, and the anonymous reviewers of our manuscript for their insightful comments which helped improve the final version significantly.

REFERENCES CITED

Arce-Burgoa, O. R., and Goldfarb, R.J., 2009, Metallogeny of Bolivia: SEG Newsletter, v. 79, p. 8-12.

Audétat, A., Gunther, D., and Heinerich, C.A., 2000, Magmatic-hydrothermal evolution in a fractionating granite: a microchemical study of the Sn-W-F-mineralized Mole Granite (Australia): Geochimica et Cosmochimica Acta, v. 64, p. 3373–3393,

Audétat, A., 2019, The metal content of magmatic-hydrothermal fluids and its relationship to mineralization potential: Economic Geology, v. 114, p. 1033-1056, doi:10.5382/econgeo.4673

Ballouard, C., Pojol, M., Boulvais, P., Branquet, Y., Tartese, R., and Vigneresse, J., 2016, Nb-Ta fractionation in peraluminous granites: A marker of the magmatic-hydrothermal transition: Geology, v. 44, p. 231-234, doi:10.1130/G37475.1

Blevin, P.L., and Chappell, B.W., 1992, The role of magma sources, oxidation states and fractionation in determining the granite metallogeny of eastern Australia: Earth and Environmental Science Transactions of the Royal Society of Edinburgh, v. 83, p. 305-316

Blevin, P.L., and Chappell, B.W., 1995, Chemistry, origin, and evolution of mineralized granites in the Lachlan Fold Belt, Australia: the metallogeny of I- and S-type granites: Economic Geology, v. 90, p. 1604-1619, https://doi.org/10.2113/gsecongeo.90.6.1604

Borisova, A.Y., Thomas, R., Salvi, S., Candaudap, F., Lanzanova, A., and Chmeleff, J., 2012, Tin and associated metal and metalloid geochemistry by femtosecond LA-ICP-QMS microanalysis of pegmatite-leucogranite melt and fluid inclusions: new evidence formelt-melt-fluid immiscibility: Mineralogical Magazine, v. 76, p. 91-113, DOI: 10.1180/minmag.2012.076.1.91

Brown, T. and Pitfield, P., 2014, In Gunn, G., ed., Critical metals handbook: Oxford, John Wiley and Sons, p. 312-339.

Burnham, C.W., and Ohmoto, H., 1980, Late-stage processes of felsic magmatism. S. Ishihara, S. Takenouchi (Eds.), Granitic Magmatism and Related Mineralization, Mineralogical Society of Canada, Victoria, British Columbia Spec., v.8, p.1-11.

Chang, Z.S., Shu, L.S., and Meinert, L.D., 2019, Skarn deposits of China: SEG Special Publications, v. 22, p. 189-234, doi: 10.5382/SP.22.06; 46 p.

Clark, A.H., Farrar, E., Kontak, D.J., Langridge, R.J., 1990, Geologic and geochronologic constraints on the metallogenic evolution of the Andes of southeastern Peru: Economic Geology, v. 85, p. 1520-1583.

Zhao, P., Chu, X., Williams-Jones, A. E., Mao, J., and Yuan, S., 2022,
The role of phyllosilicate partial melting in segregating tungsten and tin deposits in W-Sn metallogenic provinces:
Geology, v. 50, p. 121-125.

Gardiner, N.J., Hawkesworth, C.J., Robb, L.J., Whitehouse, M.J., Roberts, N.M.W., Kirkland, C.L., and Evans, N.J., 2017, Contrasting granite metallogeny through the zircon record: a case study from Myanmar: Scientific Reports, v. 7, p. 748.

Holland, T.J.B., and Powell, R., 1998, An internally consistent thermodynamic data set for phases of petrological interest: Journal of Metamorphic Geology, v. 16, p. 309-343.

Ishihara, S., 1977, The magnetite-series and ilmenite-series granitic rocks: Mining Geology, v. 27, p. 293-305

Ishihara, S., 1981, The granitoid series and mineralization, v.75, p. 458-484.

Ishihara S., Hashimoto, M., and Machida, M., 2000, Magnetite/ilmenite-series classification and magnetic susceptibility of the Mesozoic-Cenozoic batholiths in Peru: Resource Geology, v. 50, p. 123-129.

Lecumberri-Sanchez, P., Vieira, R., Heinrich, C.A., Pinto, F., and Walle, M., 2017, Fluid-rock interaction is decisive for the formation of tungsten deposits: Geology, v. 45, p. 579-582, doi:10.1130/G38974.1

Lehmann, B., 1990, Metallogeny of tin: Berlin, Springer, 211 p.

Lehmann, B., 2020, Formation of tin ore deposits: A reassessment: Lithos, 105756, doi.org/10.1016/j.lithos.2020.105756

Liu, Y.J., Li, Z.L., and Ma, D.S., 1982, Geochemistry of the tungsten-bearing Formations in South China: Science in China (Series B), v. 10, p. 939-950

Mao, J.W., Ouyang, H.G., Song, S.W., Santosh, M., Yuan, S.D., Zhou, Z.H., Zheng, W., liu, H., Liu, P., Cheng, Y.B., and Chen, M.H., 2019, Geology and metallogeny of tungsten and tin deposits in China: Economic Geology, v. 22, p. 411-482.

Miller, C.F., McDowell, S.M., and Mapes, R.W., 2003, Hot and cold granites? Implications of zircon saturation temperatures and preservation of inheritance: Geology, v. 31, p. 529-532, https://doi.org/10.1130/0091-7613(2003)031<0529:HACGIO>2.0.CO;2

Zhao, P., Chu, X., Williams-Jones, A. E., Mao, J., and Yuan, S., 2022,
The role of phyllosilicate partial melting in segregating tungsten and tin deposits in W-Sn metallogenic provinces:
Geology, v. 50, p. 121-125.

Mlynarczyk, M.S.J., and Williams-Jones, A.E., 2005, The role of collisional tectonic in the metallogeny of the Central Andean tin belt: Earth and Planetary Science Letters, v. 240, p. 656-667, doi:10.1016/j.epsl.2005.09.047

Romer, R.L., and Kroner, U., 2016, Phanerozoic tin and tungsten mineralization-tectonic controls on the distribution of enriched protoliths and heat sources for crustal melting: Gondwana Research, v. 31, p. 60-95, http://dx.doi.org/10.1016/j.gr.2015.11.002

Rudnick, R.L., and Gao, S., 2014, Composition of the Continental Crust, in Holland, H.D., ed., Treatise on Geochemistry, 2nd: Elsevier, v. 4, p. 39.

Simons, B., Andersen, J.C.Ø., Shail, R.K., and Jenner, F.E., 2017, Fractionation of Li, Be, Ga, Nb, Ta, In, Sn, Sb, W and Bi in the peraluminous Early Permian Variscan granites of the Cornubian batholith: Precursor processes to magmatic-hydrothermal mineralization: Lithos, v. 278, p. 491–512.

Sinclair, W.D., Gonevchuk, G.A., Korostelev, P.G., Semenyak, B.I., Rodionov, S., Seltmann, R., and Štemprok, M., 2011. World distribution of tin and tungsten deposits. Geological Survey of Canada, Open File 5482, Doi:10.4095/287906Xx.

Su, H.M., and Jiang, S.Y., 2017, A comparison study of tungsten-bearing granite and related mineralization in the northern Jiangxi-southern Anhui provinces and southern Jiangxi Province in South China: Science China Earth Science, v. 60, p. 1942-1958.

Watson, E.B., and Harrison, T.M., 1983, Zircon saturation revisited: Temperature and composition effects in a variety of crustal magma types: Earth and Planetary Science Letters, v. 64, p. 295-304, https://doi.org/10.1016/0012-821X(83)90211-X

White, R.W., Powell, R., and Holland, T.J.B., 2001. Calculation of partial melting equilibria in the system Na_2O-CaO-K_2O-FeO-MgO-Al_2O_3-SiO_2-H_2O (NCKFMASH): Journal of Metamorphic Geology, v. 19, p. 139-153, https://doi.org/10.1046/j.0263-4929.2000.00303.x

Zhao, P., Chu, X., Williams-Jones, A. E., Mao, J., and Yuan, S., 2022,
The role of phyllosilicate partial melting in segregating tungsten and tin deposits in W-Sn metallogenic provinces:
Geology, v. 50, p. 121-125.

White, R.W., Powell, R., and Holland, T.J.B., 2007, Progress relating to calculation of partial melting equilibria for metapelites: Journal of Metamorphic Geology, v. 25, p. 511-527, doi:10.1111/j.1525-1314.2007.00711.x.

Wolf, M., Romer, R.L., Franz, L., and López-Moro, F.J., 2018, Tin in granitic melts: the role of melting temperature and protolith composition: Lithos, v. 310-311, p. 20-30.

Yuan, S.D., Williams-Jones, A.E., Romer, R.L., Zhao, P.L., and Mao, J.W., 2019, Protolith-related thermal controls on the decoupling of Sn and W in Sn-W metallogenic province: insights from the Nanling region, China: Economic Geology, v. 114, p. 1005-1012, doi:10.5382/econgeo.4669; 8 p.

Zajacz, Z., Halter, W.E., Pettke, T., and Guillong, M., 2008, Determination of fluid/melt partition coefficients by LA-ICPMS analysis of co-existing fluid and silicate melt inclusions: Controls on element partitioning: Geochimica et Cosmochimica Acta, v. 72, p. 2169-2197, doi:10.1016/j.gca.2008.01.034

Figure and table captions

Figure 1. The global distribution of major W and Sn metallogenic belts (Sinclair et al., 2011). The relative sizes of the deposits are indicated by the sizes of the symbols. QQK denotes Qinling-Qilian-Kunlun W belt (Mao et al., 2019).

Figure 2. A: A binary plot of the bulk Fe_2O_3/FeO ratios of W and Sn granites versus their SiO_2 contents. Also shown are the fields of magnetite and ilmenite series granites taken from Ishihara et al. (2000). B: Histograms of the initial temperature of the magmas crystallizing W- and Sn-related granites in major W and Sn belts (Fig. 1), estimated using zircon saturation temperatures (see Fig. S1 and Supplementary Material 1 for further information).

Figure 3. Results of the modeling of the partial melting of an average metapelite at P=0.5 GPa. The modeling results for 0.7 and 0.9 GPa are similar to those for 0.5 GPa and are shown in Figure S2. Figure A1 shows the proportions of the phases as a function of temperature during partial melting of an average metapelite (White et al., 2007) and Figure B1 shows the proportions after extraction of 10 wt % of the melt (dashed black line), i.e., after exhaustion of muscovite in A1. Figures A2 and B2 show the evolution of the W and Sn metal fraction (wt%) in minerals and magma during partial melting. Figures A3 and B3 show the evolution of W and Sn concentrations (ppm) in the magma during partial melting. The green and grey domains denote the continuous reactions of muscovite- and biotite-dehydration melting, respectively. The stars indicate the starting melt composition for the fractionation model in Figure 4. The uncertainties propagated from the partition coefficients are presented as shadows. Details of the modeling method are provided in Supplementary Material 1. Mineral abbreviations: Bi: biotite; Cd: cordierite; Grt: garnet; ilm: ilmenite; Ksp: K-feldspar; Sill: sillimanite; Mt: magnetite; Mus: muscovite; Opx: orthopyroxene; Pl: plagioclase; Qtz: quartz.

Figure 4. The evolution of W and Sn concentrations in residual melt during fractional crystallization based on a Rayleigh fractionation model. The starting compositions of the melts were taken from the results of the partial melting model illustrated in Figure 3 (W_1, Sn_1, W_2, Sn_2, W_3, and Sn_3, as starting compositions, are indicated by the same terms in Figure 3). The solid and dashed lines correspond to the W and Sn concentrations in the initial melts derived by melting metasedimentary rocks of the Shuangqiaoshan Group in the W-Sn metallogenic belts of South China (Liu et al., 1982) and bulk continental crust (Rudnick and Gao, 2014), respectively. The W and Sn concentrations in melt inclusions (blue and pink bars) from W-Sn-related granites (Audétat et al., 2000; Zajacz et al., 2008; Borisova et al., 2012) are shown for comparison. The uncertainties propagated from the

abundance of crystallized minerals are presented as shadows. Details of the modeling method are provided in Supplementary Material 1.

Table S1. Bulk compositions of W- and Sn-related granites in the Nanling W-Sn region (1A), the Jiangnan W belt (1B), the Southeast Asian Sn belt (1C), the Youjiang Sn belt (1D), the QQK W-Sn belt (1E), the Cornwall Sn region (1F), and the Bolivian Sn belt (1G).

Table S2. Mineral-melt partition coefficients used to model partial melting.

Table S3. Results of the modeling of mineral proportions and W and Sn concentration in melts and minerals during partial melting at T = 650-1000 °C and P = 0.5, 0.7 and 0.9 GPa.

Figure S1. Zircon-saturation temperature (T_{Zr}) as a function of the fractionation indices (Nb/Ta, Zr/Hf, Rb/Sr, and TiO_2) for W- or Sn-related granites in the major W-Sn metallogenic belts shown in Figure 1. Orange diamonds refer to Sn-related granites and blue circles refer to W-related granites. For individual intrusions, the grey arrows show the trend of decreasing magma temperature with increasing degree of fractional crystallization. Therefore, the least-evolved samples for individual intrusions were considered to best represent the melting temperature for the granite. The data are from Table S1.

Figure S2. Results of the modeling of partial melting for pressures of 0.7 and 0.9 GPa. Figures A1 and B1 show the modal proportions of the phases as a function of temperature during partial melting of an average metapelite (White et al., 2007) and Figures A4 and B4 show the proportions after extraction of 10 wt% of the melt (dashed black line), i.e., after exhaustion of the available muscovite in A1 and B1. Figures A2, B2, A5 and B5 show the evolution of the W and Sn proportions (wt%) in minerals and melt during partial melting. Figures A3, B3, A6 and B6 show the evolution of W and Sn concentrations (ppm) in the magma during partial melting. The green and grey domains correspond to muscovite- and biotite-dehydration melting, respectively. Bi: biotite; Cd: cordierite; Grt: garnet; ilm: ilmenite; Ksp: K-feldspar; Sill: sillimanite; Mt: magnetite; Mus: muscovite; Opx: orthopyroxene; Pl: plagioclase; Qtz: quartz.

Figure S3. Whole-rock W or Sn concentrations as a function of the fractionation index (whole-rock TiO_2 concentration) for W- or Sn-related granites in the W-Sn metallogenic belts shown in Figure 1. For most granites, both the W and Sn concentration increase with the degree of fractional crystallization, indicating that magma evolution did not lead to the depletion of the ore metal (e.g. W or Sn) and, thus, the decoupled behavior of W and Sn mineralization. The data are from Table S1.

Figure S4. Whole-rock Fe_2O_3/FeO ratios as a function of fractionation index (whole-rock TiO_2 concentration) for W- and Sn-related granites in the W-Sn metallogenic belts shown in Figure 1. The Fe_2O_3/FeO ratios are largely independent of the degree of fractional crystallization, indicating that the redox state of the granite was inherited from the source region. The data are from Table S1.

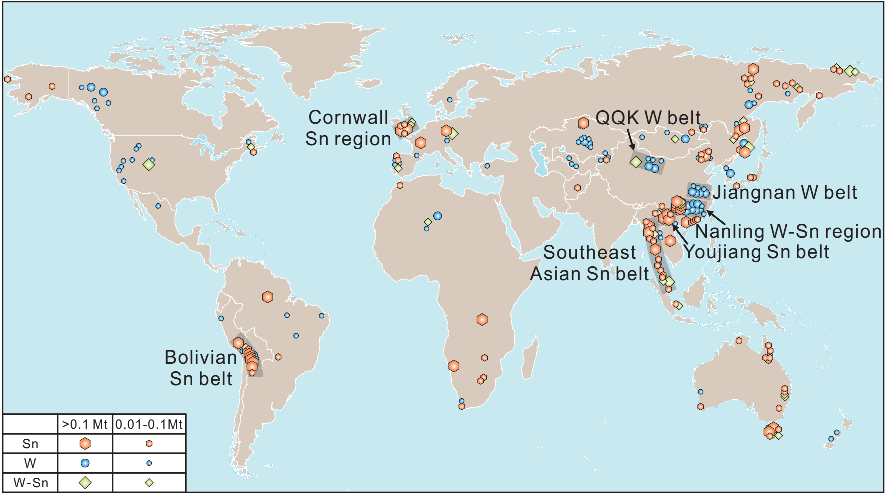

Cornwall
Sn region
QQK W belt
Jiangnan W belt
Nanling W-Sn region
Youjiang Sn belt
Southeast
Asian Sn belt
Bolivian
Sn belt
>0.1 Mt
0.01-0.1Mt
Sn
W
W-Sn

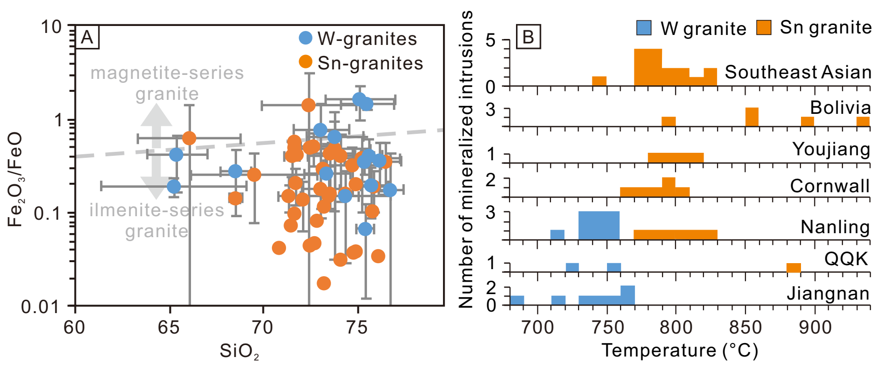

A
W-granites
Sn-granites
magnetite-series granite
ilmenite-series granite
10
1
0.1
0.01
Fe2O3/FeO
60
65
70
75
SiO2
B
W granite
Sn granite
Southeast Asian
Bolivia
Youjiang
Cornwall
Nanling
QQK
Jiangnan
Number of mineralized intrusions
5
0
3
1
2
3
1
2
0
700
750
800
850
900
Temperature (°C)

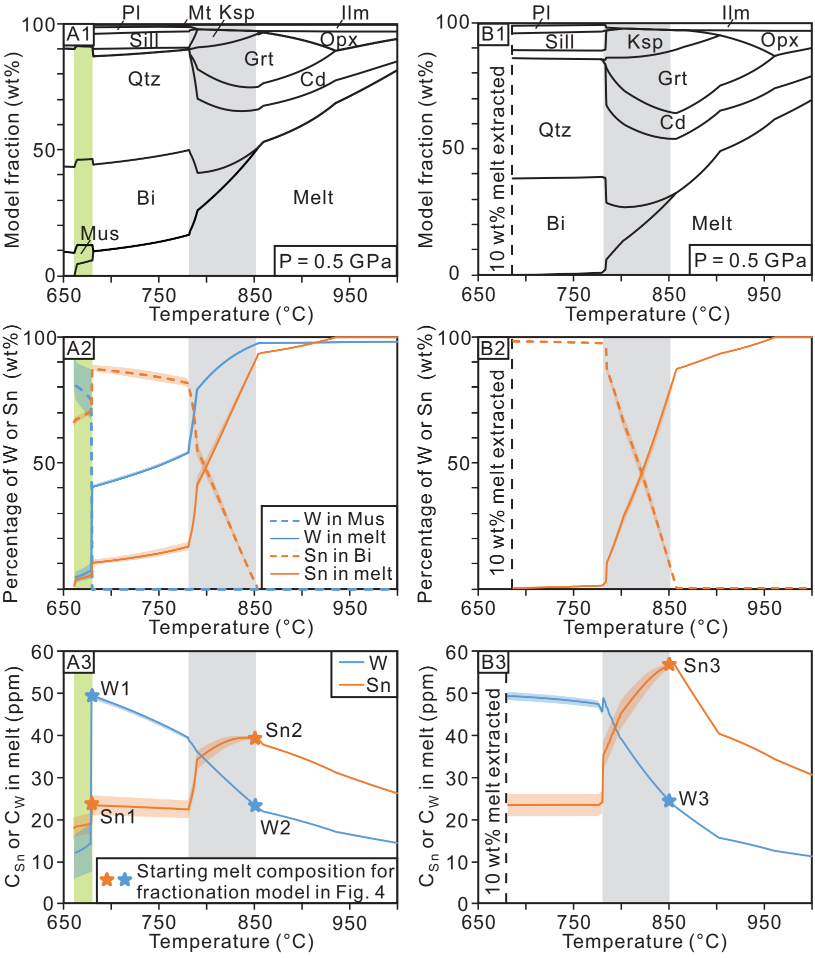
A1
Pl
Mt
Ksp
Ilm
Sill
Opx
Grt
Qtz
Cd
Bi
Melt
Mus
P = 0.5 GPa
Model fraction (wt%)
Temperature (°C)
B1
Pl
Ilm
Sill
Ksp
Opx
Grt
Qtz
Cd
Bi
Melt
10 wt% melt extracted
P = 0.5 GPa
Model fraction (wt%)
Temperature (°C)
A2
W in Mus
W in melt
Sn in Bi
Sn in melt
Percentage of W or Sn (wt%)
Temperature (°C)
B2
10 wt% melt extracted
Percentage of W or Sn (wt%)
Temperature (°C)
A3
W
Sn
W1
Sn1
Sn2
W2
Starting melt composition for fractionation model in Fig. 4
C_{Sn} or C_W in melt (ppm)
Temperature (°C)
B3
Sn3
W3
10 wt% melt extracted
C_{Sn} or C_W in melt (ppm)
Temperature (°C)

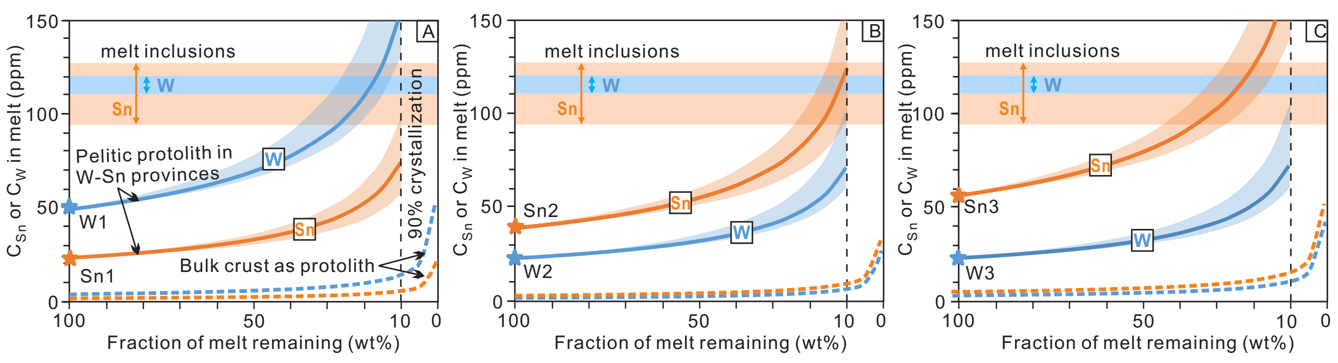

A
B
C
melt inclusions
W
Sn
Pelitic protolith in
W-Sn provinces
W1
Sn1
Bulk crust as protolith
90% crystallization
Sn2
W2
Sn3
W3
C_{Sn} or C_W in melt (ppm)
Fraction of melt remaining (wt%)
150
100
50
0
100
50
10
0